Research in Astron. Astrophys. **2011** Vol. **11** No. **4**, 445–456
http://www.raa-journal.org *http://www.iop.org/journals/raa*

Research in Astronomy and Astrophysics

The multiwavelength emission from the gamma-ray binary LS I + 61 303 *

Jian-Fu Zhang[1], Ya Zhu[1] and Li Zhang[2]

[1] Department of Physics and Electronic Science, Tongren University, Tongren 554300, China; *jianfuzhang.yn@gmail.com*
[2] Department of Physics, Yunnan University, Kunming 650091, China

Received 2010 September 20; accepted 2010 December 10

Abstract This paper presents a hadronic dominated jet model to investigate multi-wavelength emission from the microquasar LS I + 61 303. In this scenario, we take into account evolutions of the primary particles and secondary $e^{\pm}$ pairs; these pairs are produced by the collisional interactions of the accelerated protons with the cold jet protons and the stellar wind ions. In this model, the non-thermal photons are produced by π^0 decay emission, synchrotron and inverse Compton scattering processes from the primary electrons and secondary pairs, and relativistic bremsstrahlung emission from the secondary leptonic pairs. Based on this model framework, we show that the spectral energy distributions can be produced by the primary and secondary particles via interactions with the cold matter, and magnetic and stellar radiation fields. We also consider the attenuation of angular dependence γ-γ due to the effects of the stellar target photon fields. The resulting model can approximately reproduce the recent quasi-simultaneous observational data points and the non-simultaneous multi-band observations.

Key words: radiation mechanism: non-thermal — gamma rays: general — X-ray: binaries — stars: individual: LS I + 61 303

1 INTRODUCTION

LS I + 61 303 is one of the microquasar candidates which is a Galactic X-ray binary system with relativistic radio jets (Mirabel & Rodríguez 1999). Microquasars are comprised of a non-degenerate stellar object, which can experience different stages of its evolution, and a central compact object, which can be a neutron star or a black-hole candidate. According to the mass of the non-degenerate stellar companion, microquasars can be divided into a high-mass microquasar and a low-mass one. It is thought that the compact object powers the relativistic jets with non-thermal emission through accretion of the matter expelled from the companion, which forms an accretion disk that is usually detected in X-ray wavelengths.

There are two kinds of models to describe the non-thermal emission from microquasars: leptonic or hadronic origin. In the leptonic model, steady-state (e.g. Bosch-Ramon et al. 2006a; Zhang et al. 2009) and time-dependent (e.g. Gupta & Böttcher 2006) emission models have been proposed.

* Supported by the National Natural Science Foundation of China.

In the steady-state case, the jet can be modeled as dynamically dominated by cold protons and radiatively dominated by relativistic leptons; the characteristics of the orbit and companion star constrain the way in which accretion occurs (e.g. Bosch-Ramon et al. 2006a). In the time-dependent case, Gupta & Böttcher (2006) have investigated the synchrotron and inverse Compton (IC) signatures of time-dependent electron injection and acceleration, and adiabatic and radiative cooling processes by considering different jet geometries for microquasars. In the hadronic model, the relativistic protons in the jet interact with target protons from outside of the jet (the stellar wind of the companion star and the surrounding interstellar matter) and from the jet itself, via p-p and/or p-γ interactions (e.g. Romero et al. 2003; Romero et al. 2005; Christiansen et al. 2006; Orellana et al. 2007; Romero & Vila 2008; Zhang et al. 2010; Zhang & Feng 2010).

Concretely, Romero et al. (2003) developed a model of the hadronic γ-ray emission from windy microquasars. Furthermore, they also investigated the hadronic high-energy γ-ray emission from the microquasar LS I + 61 303 before the TeV emission was observed in this source (Romero et al. 2005). Recently, Orellana et al. (2007) have calculated the leptonic secondary emission in a hadronic microquasar model via considering a simplified geometry of a circular orbit and spherical wind for a massive microquasar. However, a comparison study between a multiwavelength emission model using a hadronic dominated jet model and simultaneous or non-simultaneous multiwavelength observations has not yet been found. Therefore, we present this work to investigate the multiwavelength emission of LS I + 61 303. Comparing the predicted spectral energy distributions (SEDs) with the high-confidence data points available at the two orbital-phase points, we hope to study whether a hadronic jet model can explain the multiwavelength emissions from this source.

In this paper, we put forward a hadronic dominated jet model from the microquasar LS I + 61 303 via introducing a parameter ($\gg$1) that is the ratio of the relativistic primary electron to proton power. Under this model framework, we study the multiwavelength emission of this typical binary source by considering evolutions of the primary particles and secondary $\mathrm{e}^{\pm}$ pairs; these pairs are produced via p-p collisions due to the accelerated protons in the jet interacting with the stellar wind and cold jet matter. Adopting the improved parameterized formulae for p-p interactions and the recent orbital geometry of the microquasar LS I + 61 303 we present the notion that the SEDs can be produced by the primary and secondary particles interacting with the cold matter, and magnetic and stellar photon fields. Furthermore, we take into account the attenuation of the angular dependent high energy γ-photon due to the effects of the stellar target photon fields. The resulting model can approximately reproduce the available quasi-simultaneous observational data and the non-simultaneous observations.

The outline of this work is organized as follows. We present a description of the model in Section 2; the numerical results from the microquasar LS I + 61 303 in Section 3; and discussion and conclusions in Section 4.

2 MODEL DESCRIPTION

In this section, we describe a basic scenario of the jet model for the microquasar LS I + 61 303. We then present all kinds of radiative processes (from primary and secondary particles) and absorptive processes (due to high energy γ-rays interacting with stellar photon fields).

2.1 Basic Scenario of the Jet Model

In our model, the magnetic-hydrodynamical mechanism for the jet ejection is assumed to operate in the microquasar LS I + 61 303 via converting magnetic energy into matter kinetic energy. We also assume that the conical jets are launched perpendicularly to the orbital plane of the binary system, at a distance z_0 and with an initial radius $R_0 = z_0 \tan\zeta$, where $\zeta \approx 6^\circ$ is a half-opening angle, z_0 is the distance from the central compact object and is given as $z_0 = 50R_{\rm Sch}$ with $R_{\rm Sch} = 2GM_{\rm co}/c^2$.

Adopting the disk-jet coupling hypothesis formulated by Falcke & Bierman (1995), the total kinetic power of each jet $L_{\rm jet} = q_{\rm jet} L_{\rm acc}$ is fixed to be proportional to the accretion power onto the compact object $L_{\rm acc} = \dot{M}_{\rm acc} c^2$; here, $q_{\rm jet}$ is a parameter which equals 0.1 (Falcke & Biermann 1995; Körding et al. 2006). A fraction of this power is in the form of the relativistic primary particle $L_{\rm rel} = q_{\rm rel} L_{\rm jet}$, which includes both leptonic and hadronic contents, $L_{\rm rel} = L_{\rm p} + L_{\rm e}$, and other types of cold particles. The ratio relation between electron and proton power is depicted by a parameter $R_{\rm ep}$ in such a way that $L_{\rm e} = R_{\rm ep} L_{\rm p}$.

At the initial point of the jet ejection, the magnetic field is assumed to be lower than the equipartition level of jet matter, in contrast to the model with the cold-matter dominated jets (Bosch-Ramon et al. 2006a). Therefore, we can estimate the magnetic field strength at the ejection point as

$$B_0 = \sqrt{\chi 8\pi U_0}, \tag{1}$$

where $U_0 = L_{\rm jet}/\pi R_0^2 \upsilon_{\rm B}$ is the jet energy density, and $\upsilon_{\rm B}$ is the bulk velocity of the jet. The outflow of jet matter is supposed to expand adiabatically, therefore, the magnetic field strength $B(z)$ along the jet is considered to be $B(z) = B_0(z_0/z)$.

The source LS I + 61 303 presents a circumstellar disk (Frail & Hjellming 1991). As for the stellar wind that provides a proton target, we combine two scenarios: a disk-wind type with a circumstellar disk at smaller jet scales and another radiatively driven wind type at larger jet scales, compared to the previous works (Romero et al. 2003; Romero et al. 2005). The stellar companion of a B-type primary with wind forms a circumstellar outflowing disk with density $\rho_{\rm w}(R) = \rho_0 (R/R_\star)^{-n}$ (Gregory & Neish 2002). Through solving the continuity equation, a wind velocity $\upsilon_{\rm w} = \upsilon_0 (R/R_\star)^{n-2}$ can be obtained, which is valid in the region surrounding the equatorial plane; this wind type can be confined to a disk with half-opening angle $\vartheta = 15^\circ$ with $n = 3.2$, ρ_0 =10^{-11} g cm^{-3} and υ_0 =5 km s^{-1} (Martí & Paredes 1995). In addition, for simplicity, we consider a radiatively driven wind outside the circumstellar disk, which is given by $\upsilon(R) = \upsilon_\infty (1 - R_\star/R)^\delta$ (Lamers & Cassinelli 1999) where $R_\star$ is the stellar radius, $\upsilon_\infty \approx 2.5 \times 10^8$ cm s^{-1} is the terminal wind velocity and $\delta = 1$ is a parameter for massive stars. With a gas dominated by protons, we obtain the cold proton density along the jet axis

$$n_{\rm w}(z) = \frac{\dot{M}_\star}{4\pi m_{\rm p} \upsilon_\infty (z^2 + R_{\rm orb}^2)} \Big(1 - \frac{R_\star}{\sqrt{z^2 + R_{\rm orb}^2}}\Big)^{-\delta}, \tag{2}$$

where $\dot{M}_\star$ is the mass loss rate for a stellar companion, $R_{\rm orb}$ is the orbital radius of the binary system and $m_{\rm p}$ is the mass of a proton.

We consider the notion that the wind protons from the stellar companion laterally penetrate the jets, which results in the production of charged and neutral pions via the inelastic p-p collisions. These neutral pions immediately decay to γ-rays, whereas the charged ones decay to muons, and subsequently to electron-positron pairs. Moreover, we introduce a parameter $\kappa = 0.3$ to express the mixed extent between wind matter and jet particles in a phenomenological way similar to the previous works (Orellana et al. 2007).

The spectral distributions of the relativistic electrons and protons are described by a power law distribution in the form

$$N_{\rm e,p}(E_{\rm e,p}) = K_{\rm e,p} E_{\rm e,p}^{-\alpha_{\rm e,p}} \exp(-E_{\rm e,p}/E_{\rm e,p,max}),$$

in the jet reference frame; $E_{\rm e,p}$ is the energy of the particles. In our scenario, we consider that the exponent $\alpha_{\rm e,p}$ is different for the electrons and protons. Since the conical jet flow expands adiabatically, the corresponding particle flux evolves with the distance z as

$$J_{\rm e,p}(E_{\rm e,p}, z) = K_{\rm e,p} (c/4\pi)(z_0/z)^2 E_{\rm e,p}^{-\alpha_{\rm e,p}} \exp(-E_{\rm e,p}/E_{\rm e,p,max})$$

in the same frame. Using relativistic invariance, the particle flux in the observer's reference frame becomes

$$J_{\rm e,p}(E_{\rm e,p},z,\theta)=\frac{cK_{\rm e,p}}{4\pi}\left(\frac{z_0}{z}\right)^2\frac{\Gamma^{-\alpha_{\rm e,p}+1}E_{\rm e,p}^{'-\alpha_{\rm e,p}}\exp(-E_{\rm e,p}^{'}/E_{\rm e,p,max})}{\sqrt{\sin^2\theta+\Gamma^2\left(\cos\theta-\frac{\beta_{\rm b}E_{\rm e,p}}{\sqrt{E_{\rm e,p}^2-m_{\rm e,p}^2c^4}}\right)^2}}, \tag{3}$$

where $E_{\rm e,p}^{'}=E_{\rm e,p}-\beta_{\rm b}\sqrt{E_{\rm e,p}^2-m_{\rm e,p}^2c^4}\cos\theta$ is the particle energy in the frame comoving with the jet, θ is the angle subtended by the jet axis z and the motion direction of an emerging photon, Γ is the jet bulk Lorentz factor and $\beta_{\rm b}$ is the jet velocity in light velocity units c. Normalization constant $K_{\rm e,p}$ can be determined by the balance equation as follows:

$$\frac{L_{\rm rel}}{\pi R_0^2c}=K_{\rm p}\int_{E_{\rm p,min}}^{E_{\rm p,max}}E_{\rm p}^{-\alpha_{\rm p}}E_{\rm p}dE_{\rm p}+K_{\rm e}\int_{E_{\rm e,min}}^{E_{\rm e,max}}E_{\rm e}^{-\alpha_{\rm e}}E_{\rm e}dE_{\rm e}. \tag{4}$$

In this work, we assume that the minimum energies are $E_{\rm p,min}\approx$1 GeV and $E_{\rm e,min}\approx$1 MeV for the proton and electron, respectively. The maximum energy of the proton can be determined by the equality between the size of the accelerator and the maximum proton gyroradius; the former is considered as the jet radius, namely, $E_{\rm p,max}=QR_{\rm jet}(z_0)B(z_0)$ with $R_{\rm jet}(z)=z{\rm tan}\zeta$ where Q is the charge of a particle. The maximum energy of the primary electron can be obtained by balancing the acceleration rate with the total radiative and adiabatic loss rates at the base of the jet. The SEDs of primary electrons and protons are presented in Figure 1, using $R_{\rm ep}=2\times10^{-4}$, $\chi=10^{-6}$, $\alpha_{\rm e,p}=2$, $q_{\rm rel}=0.1$ and $\dot{M}_{\rm acc}=5\times10^{-9}\,M_\odot$ yr^{-1}. For a first-order approximation, we assumed that the primary electrons are not accelerated along the jet like the secondary $\rm e^{\pm}$ pairs in a phenomenological way; the re-accelerated processes of secondary particles and primary electrons accelerated simultaneously will be presented in future work. In this paper, an internal shock model in the X-ray binary jets was proposed to explain a flat radio spectrum (Jamil et al. 2010). In the following section, we present some expressions of various cooling processes and the acceleration rate used in this work.

The synchrotron radiation cooling rate for a particle of energy E and mass m in a region with the magnetic field $B(z)$ is given as

$$\frac{dE}{dt}\Big|_{\rm syn}=-\frac{4}{3}\Big(\frac{m_{\rm e}}{m}\Big)^3\frac{c\sigma_{\rm T}B(z)^2}{m_{\rm e}^2c^4 8\pi}E^2, \tag{5}$$

where $\sigma_{\rm T}$ is the Thomson cross section.

The inelastic p-p collision rate of relativistic protons with the density $n_{\rm c}(z)$ is expressed by

$$\frac{dE}{dt}\Big|_{\rm pp}=-n_{\rm c}(z)c\sigma_{\rm pp}(E)K_{\rm pp}, \tag{6}$$

where $n_{\rm c}(z)=n_{\rm w}(z)+n_{\rm in}(z)$ includes the densities of both $n_{\rm w}(z)$ laterally penetrating the jet from the stellar wind and $n_{\rm in}(z)$ inside the jet; the cold proton density inside the jet is

$$n_{\rm in}(z)=\frac{(1-q_{\rm rel})L_{\rm jet}}{\Gamma m_{\rm p}c^2\pi R_{\rm jet}^2(z)\upsilon_{\rm B}}, \tag{7}$$

where $n_{\rm w}(z)$ is given by Equation (2), and the cross section for inelastic p-p interactions $\sigma_{\rm pp}(E_{\rm p})$ is approximated by equation (79) in Kelner et al. (2006), with the inelasticity coefficient $K_{\rm pp}\approx$ 1/2.

The adiabatic loss rate of a particle with an energy E is given by Bosch-Ramon et al. (2006a)

$$\frac{dE}{dt}\Big|_{\rm exp}=-\frac{2}{3}\frac{\upsilon_{\rm B}}{z}E. \tag{8}$$

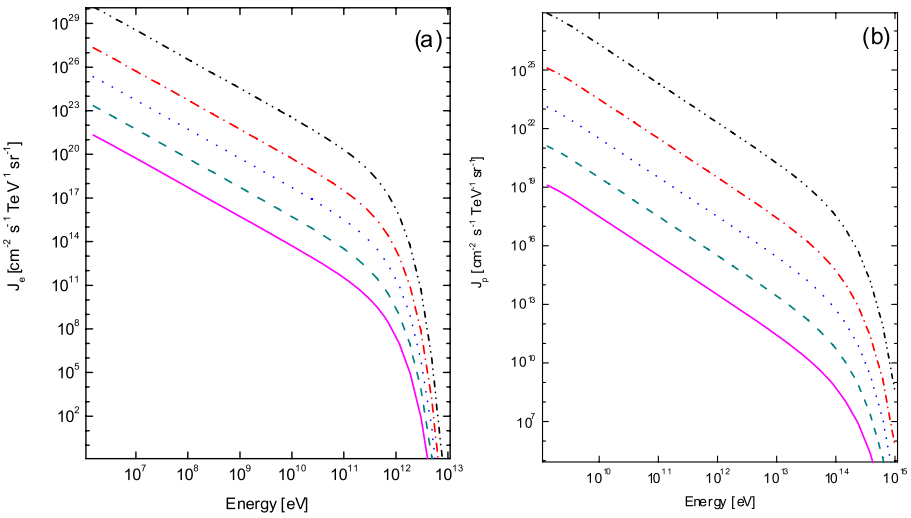

Fig. 1 SEDs of electrons $J_{\rm e}(E_{\rm e})$ (a) and those of protons $J_{\rm p}(E_{\rm p})$ (b). The corresponding spectra are plotted at $z = z_0$ (*black line*), $z = 10^9$ cm (*red line*), $z = 10^{10}$ cm (*blue line*), $z = 10^{11}$ cm (*dark cyan line*), $z = 10^{12}$ cm (*magenta line*) for the parameters $R_{\rm ep} = 2 \times 10^{-4}$, $\chi = 10^{-6}$, $\alpha_{\rm e,p} = 2$, $q_{\rm rel} = 0.1$ and $\dot{M}_{\rm acc} = 5 \times 10^{-9}\ M_\odot\ {\rm yr}^{-1}$.

The formula for the IC energy loss rate in both the Thomson and Klein-Nishina regimes can be approximated as (e.g. Bosch-Ramon & Khangulyan 2009; Araudo et al. 2009)

$$\frac{dE}{dt}\Big|_{\rm IC} = -\left(\frac{U_{\rm ph}(z)}{6.1\times10^{12}E_{\rm soft}}\right)\left(\frac{\ln(1+0.2\lambda)}{1+8.3\lambda}\right)\left(\frac{1+0.5\lambda+1.3\lambda^2}{1+1.3\lambda^2}\right)E, \tag{9}$$

where $U_{\rm ph}(z)$ is the energy density of the photon field from the stellar companion, λ=$E_{\rm soft}E/(m_{\rm e}^2c^4)$ is a parameter, and $E_{\rm soft} \approx KT$ is the typical energy of the soft photon field of the blackbody-like distribution; here, K and T are the Boltzmann constant and the effective temperature of the stellar companion respectively.

The loss rate from the bremsstrahlung emission of the relativistic lepton is expressed as

$$\frac{dE}{dt}\Big|_{\rm B} = -\frac{3\alpha_{\rm f}}{\pi}n_{\rm c}(z)c\sigma_{\rm T}\times\left[\ln\left(\frac{E}{m_{\rm e}c^2}\right)+0.36\right]E, \tag{10}$$

where $\alpha_{\rm f}$ is the fine-structure constant.

The acceleration rate for a particle of energy E in a magnetic field with strength $B(z)$ is expressed by $\dot{E}_{\rm gain}(E,z) \approx \eta cQB(z)$; η is treated here as a free parameter.

2.2 Radiative and Absorptive Processes

We consider four radiative processes of relativistic particles in all kinds of fields, which include inelastic p-p collisions of primary protons with the total target protons, synchrotron and IC processes of primary electrons and secondary $\rm e^{\pm}$ pairs, and relativistic bremsstrahlung emission of the secondary $\rm e^{\pm}$ pairs.

For the processes of inelastic p-p interactions, we adopt a series of accurate parameterized formulae to calculate spectra of various secondary particles, which greatly speed up the calculations involving p-p interaction processes in our numerical calculation. These functional formulae reproducing the secondary particle spectra include the non-diffractive, diffractive and resonance-excitation

components. The differential cross section for secondary particles can be given as (Kamae et al. 2006)

$$\frac{d\sigma(E_{\rm p},E_{\rm sec})}{dE_{\rm sec}} = \frac{d\sigma_{\rm ND}(E_{\rm p},E_{\rm sec})}{dE_{\rm sec}} + \frac{d\sigma_{\rm diff}(E_{\rm p},E_{\rm sec})}{dE_{\rm sec}} + \frac{d\sigma_{\triangle(232)}(E_{\rm p},E_{\rm sec})}{dE_{\rm sec}} + \frac{d\sigma_{\rm res1600}(E_{\rm p},E_{\rm sec})}{dE_{\rm sec}}. \quad (11)$$

Then, the luminosity of the total γ-ray spectra is expressed as

$$L_\gamma = E_\gamma^2 \int \pi R_{\rm jet}(z)^2 n_{\rm c}(z) \int \frac{4\pi}{c} J_{\rm p}(E_{\rm p},z,\theta) c \frac{d\sigma(E_{\rm p},E_\gamma)}{dE_\gamma} dE_{\rm p} dz. \quad (12)$$

The spectral distribution of secondary $\rm e^{\pm}$ pairs is given by

$$Q_{\rm e^{\pm}}(E,z) = Q_{\rm e^{+}}(E,z) + Q_{\rm e^{-}}(E,z), \quad (13)$$

where

$$Q_{\rm e^{+}}(E,z) = n_{\rm c}(z) \int \frac{4\pi}{c} J_{\rm p}(E_{\rm p},z,\theta) c \frac{d\sigma(E_{\rm p},E_{\rm e^{+}})}{dE_{\rm e^{+}}} dE_{\rm p}, \quad (14)$$

$$Q_{\rm e^{-}}(E,z) = n_{\rm c}(z) \int \frac{4\pi}{c} J_{\rm p}(E_{\rm p},z,\theta) c \frac{d\sigma(E_{\rm p},E_{\rm e^{-}})}{dE_{\rm e^{-}}} dE_{\rm p}. \quad (15)$$

These secondary particles will evolve along the jet. The steady-state secondary $\rm e^{\pm}$ spectra are shaped by the injection and cooling processes, and are governed by

$$\frac{\partial}{\partial E_{\rm e^{\pm}}}[\dot{E}_{\rm e^{\pm}}(E_{\rm e^{\pm}},z) N_{\rm e^{\pm}}(E_{\rm e^{\pm}},z)] = Q_{\rm e^{\pm}}(E_{\rm e^{\pm}},z), \quad (16)$$

where the total cooling rate is

$$\dot{E}_{\rm e^{\pm}}(E_{\rm e^{\pm}},z) = \dot{E}_{\rm syn}(E_{\rm e^{\pm}},z) + \dot{E}_{\rm exp}(E_{\rm e^{\pm}},z) + \dot{E}_{\rm B}(E_{\rm e^{\pm}},z) + \dot{E}_{\rm IC}(E_{\rm e^{\pm}},z).$$

The analytical solution to Equation (16) can be expressed as (Dolag & Enßlin 2000)

$$N_{\rm e^{\pm}}(E_{\rm e^{\pm}},z) = \frac{1}{|\dot{E}_{\rm e^{\pm}}(E_{\rm e^{\pm}},z)|} \int_{E_{\rm e^{\pm}}}^{E_{\rm e^{\pm},max}} dE'_{\rm e^{\pm}} Q_{\rm e^{\pm}}(E'_{e^{\pm}},z). \quad (17)$$

As for the synchrotron emission and IC scattering of the primary electrons and secondary $\rm e^{\pm}$ pairs, and the relativistic bremsstrahlung emission of the secondary $\rm e^{\pm}$ pairs, we use the classical formulae from Blumenthal & Gould (1970). The SEDs produced in the various interaction processes are transformed into the observer's reference frame.

The radiation field of the stellar companion provides a suitable target for the absorption of high-energy γ-ray photons. Dubus (2006) has investigated the γ-ray absorption in massive X-ray binaries (i.e. LS 5039, PSR B1259–63 and LS I + 61 303) via taking the spectral distribution, orbital modulation and finite size of the stellar companion into account. Böttcher & Dermer (2005) have studied the γ-γ absorptions of very high-energy γ-rays from microquasars via considering the stellar companion as a point-like source. In our calculation, we adopt the latter case because the point-like source approximation method is accurate enough in our scenario.

3 NUMERICAL RESULTS

LS I + 61 303 is a high-mass X-ray binary system with a circumstellar disk located at a distance of $\approx$ 2 kpc. The other parameters of this source are listed in Table 1. The accretion nature of LS I + 61 303 is still unclear, although some works considering this source as an accreting microquasar have been done (see, e.g. Bosch-Ramon et al. 2006b; Romero et al. 2007). In our calculation, the change in accretion rate with an elliptical orbit is treated as a free parameter. Moreover, the other free parameters such as $q_{\rm rel}$, χ and $R_{\rm ep}$ are respectively fixed to 0.1, 10^{-6} and 2×10^{-4} within their reasonable parameter ranges.

The SEDs of various radiation processes at the superior conjunction point are shown in Figure 2. They include π^0 decay emission, synchrotron and IC scattering components of the primary electrons and secondary $\rm e^{\pm}$ pairs, relativistic bremsstrahlung emission of the secondary $\rm e^{\pm}$ pairs and target photon fields from the companion star.

Table 1 Fixed Parameters for LS I + 61 303

Parameter	Value	Unit	Reference
Orbital semi-major axis	$\sim 5 \times 10^{12}$	cm	[1]
Be primary star luminosity	2×10^{38}	erg $\rm s^{-1}$	[1]
Compact object mass	2.67	$M_\odot$	[1]
Surface temperature of stellar companion	2.8×10^4	K	[1]
Orbital period	26.4960	d	[2]
Orbital eccentricity	0.537	–	[3]
Bulk Lorentz factor	1.25	–	[4]

[1] Casares et al. (2005); [2] Gregory (2002); [3] Aragona et al. (2009); [4] Massi et al. (2004).

As shown in Figure 2, at the optical-ultraviolet wavebands, the thermal radiation from the stellar companion's photon fields dominates emission output. The emissions in the radio and from the soft X-rays to $\sim$ 1 GeV ranges are mainly produced by the synchrotron emission of the primary electrons and secondary $\rm e^{\pm}$ pairs. From this figure, it is apparent that the luminosity at $\sim$ 10 MeV is $\sim 10^{35}$ erg $\rm s^{-1}$. At high-energy γ-ray wave bands, dominant emissions are π^0 meson decay emission and IC scattering of the primary and secondary $\rm e^{\pm}$ pairs. However, the contributions to the relativistic bremsstrahlung emission of the secondary particles can be neglected. The emission in very high-energy γ-rays is dominated by the π^0 decay emission. Attenuation of the non-thermal high-energy photons due to absorption in the stellar photon fields is taken into account for the total spectrum (thick solid line) in our calculation. We can find that the total energy spectrum presents a plateau at about the TeV regions.

To reproduce the SEDs of LS I + 61 303 related to the orbital modulations, we adopt the different spectral indices of particles and the different accretion rates into the central compact object from the stellar companion at two orbital phases. We calculate the emission spectrum of the microquasar LS I + 61 303 (see Figs. 3 and 5) at the inferior conjunction (INFC) $\Psi = 0.313$ (Aragona et al. 2009), which can approximately reproduce the latest *Fermi* Large Area Telescope (LAT) data (Abdo et al. 2009) and radio data points (Albert et al. 2008). In addition, we compute the SEDs (see Figs. 4 and 5) at phase $\Psi = 0.775$ (Aragona et al. 2009), which can approximately match the flux values from the Major Atmospheric Gamma Imaging Cherenkov telescope (MAGIC) X-ray and soft γ-ray observations (MAGIC: Albert et al. 2009; OSSE: Strickman et al. 1998; SAX-PDS: Sidoli et al. 2006; COMPTEL: van Dijk et al. 1996) near the apastron passage.

Figure 3 (Fig. 4) illustrates that there is a general agreement between the observed data and our numerical results for LS I + 61 303 at the INFC (apastron passage). As indicated in Figure 3 (i.e. at the INFC), the radio (Albert et al. 2009), X-ray (OSSE: Strickman et al. 1998) and soft γ-ray (COMPTEL: van Dijk et al. 1996) observations can mainly be produced by the synchrotron emission

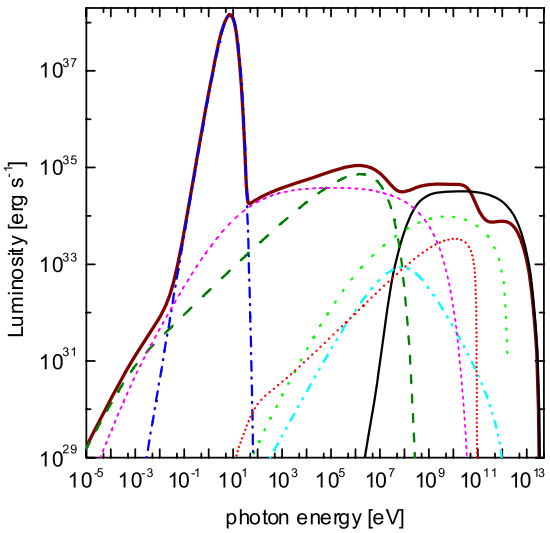

Fig. 2 Resulting multiwavelength spectra given by the hadronic dominated jet model with $\alpha_{\rm e,p} = 2$ and $\dot{M}_{\rm acc} = 5 \times 10^{-9}\ M_\odot\ {\rm yr}^{-1}$ at the superior conjunction point $\Psi = 0.081$. In the figure, we show the π^0 decay emission (*black line*), the synchrotron emission (*olive line*) and IC scattering (*red line*) of the primary electrons, and the synchrotron (*magenta line*), relativistic bremsstrahlung (*cyan line*) and IC processes (*green line*) of the secondary $e^{\pm}$ pairs, the blackbody radiation of the stellar (*blue line*) and the total emission spectrum (*thick wine line*).

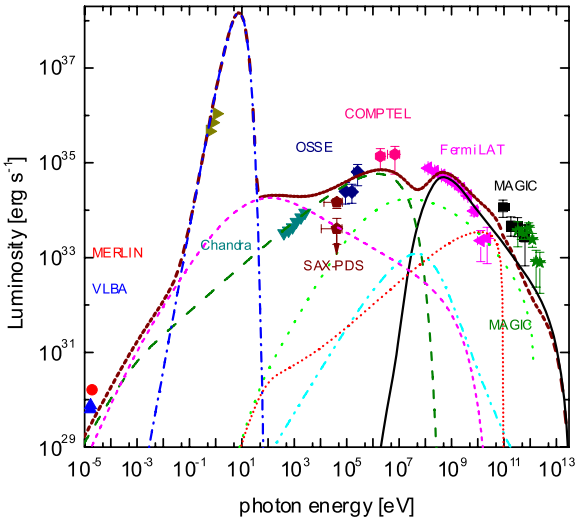

Fig. 3 Multiwavelength spectra of LS I + 61 303 reproduced at the inferior conjunction (INFC) point Ψ=0.313 (*thick wine line*). The quasi-simultaneous observational radio, Chandra and MAGIC data points (*filled square*)(Albert et al. 2008), the non-simultaneous observational OSSE (Strickman et al. 1998) SAX-PDS (Sidoli et al. 2006), COMPTEL (van Dijk et al. 1996), *Fermi* LAT (Abdo et al. 2009) and MAGIC (*filled pentagram*) (Albert et al. 2009) points are indicated. The adopted parameters are $\alpha_{\rm e} = 2$, $\alpha_{\rm p} = 2.7$ and $\dot{M}_{\rm acc} = 4.4 \times 10^{-9}\ M_\odot\ {\rm yr}^{-1}$. Other corresponding descriptions are the same as those in Fig. 2.

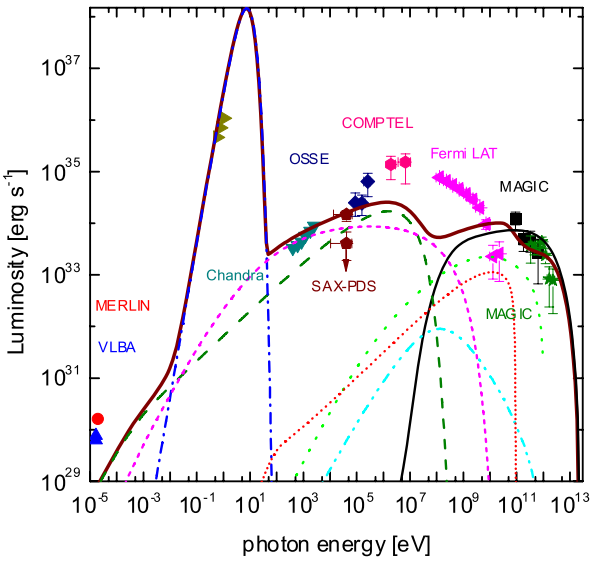

Fig. 4 Multiwavelength SEDs of LS I + 61 303 reproduced at the apastron passage Ψ=0.775 (*thick wine line*). The illustrations of observational points are the same as those in Fig. 3. The adopted parameters are $\alpha_{\rm e} = 2$, $\alpha_{\rm p} = 1.9$ and $\dot{M}_{\rm acc} = 2.2\times10^{-9}\ M_{\odot}\ {\rm yr}^{-1}$. Other corresponding descriptions are the same as those in Fig. 2.

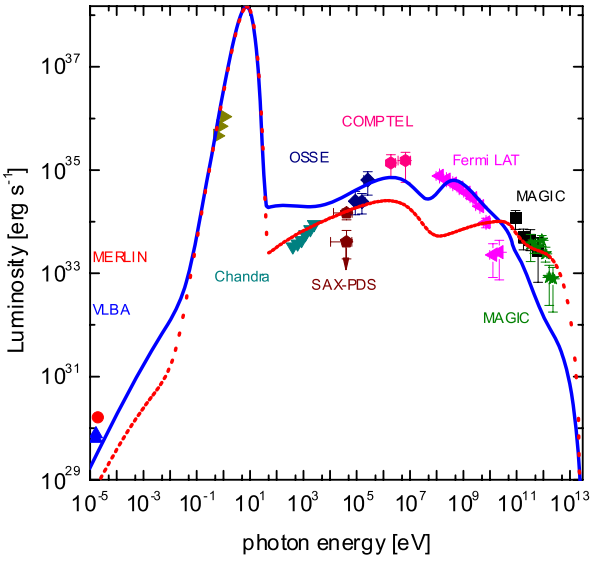

Fig. 5 Multiwavelength spectra of LS I + 61 303 at two orbital phases of the inferior conjunction (INFC) Ψ=0.313 (*thick blue line*) and apastron passage Ψ=0.775 (*thick red line*). The illustrations of observational points are the same as those in Fig. 3. The adopted parameters are the same as those in Fig. 3 at the INFC, and those in Fig. 4 at the apastron passage.

of primary and secondary leptons; there is little contribution from the IC scattering of the secondary $e^{\pm}$ pairs at the soft γ-ray wave bands. The *Fermi* LAT observational data points (Abdo et al. 2009) are reproduced by the π^0 decay emission and IC scattering of the secondary pairs. At very high-energy γ-ray bands, the resulting flux value is lower than the observed flux from the TeV detectors, which is consistent with the recent TeV observation showing no emission signature close to periastron passage (Albert et al. 2008). As shown in Figure 4 (i.e. at the apastron passage), although the resulting radio flux is lower than the obtained observations from the Multi-Element Radio Linked Interferometer (MERLIN) and Very Long Baseline Array (VLBA) (Albert et al. 2008), the total emission spectrum can synchronously reproduce the observations from the X-ray (Chandra: Albert et al. 2008) and TeV (Albert et al. 2009) energy regions.

For clarity, we have removed all the individual emission components and only presented the total SEDs absorbed by the γ-γ interactions in Figure 5. The radio emission luminosity that is produced by the synchrotron emission of the primary electrons and secondary $e^{\pm}$ pairs is slightly lower than the observed one. From the optical to ultraviolet wavelengths, the emission component is the thermal radiation from the stellar companion. Furthermore, the synchrotron emission spectra of primary and secondary pairs and the IC scattering spectrum of the secondary pairs can approximately reproduce the observational data points from Chandra (Albert et al. 2008), SAX-PDS (Sidoli et al. 2006), OSSE (Strickman et al. 1998) and COMPTEL (van Dijk et al. 1996). The π^0 decay emission and IC interaction processes can also approximately explain observations from the *Fermi* LAT (Abdo et al. 2009) and MAGIC (Albert et al. 2008).

4 DISCUSSION AND CONCLUSIONS

Up to now, there are some studies in the literature discussing the different possibilities concerning the nature of LS I + 61 303, i.e. the accreting microquasars vs the non-accreting pulsar binaries (e.g. Martocchia et al. 2005; Dubus 2006; Bosch-Ramon et al. 2006a; Chernyakova et al. 2006; Romero et al. 2007; Bosch-Ramon & Khangulyan 2009). In this work, we have treated LS I + 61 303 as a microquasar. On the premise of the treatment, this work presented a hadronic dominated jet model of the source LS I + 61 303, taking into account the evolutions of primary particles and secondary $e^{\pm}$ pairs. In our model, we calculated the SEDs of the primary and secondary particles and considered the attenuation of high-energy γ-photons due to the existence of the stellar target photon fields.

Although the SEDs predicted at phase 0.313 (see Fig. 3) can reproduce the OSSE data (Strickman et al. 1998) and the *Fermi* LAT data (Abdo et al. 2009), the model does not fit the Chandra X-ray data; furthermore, radio and TeV data also seem higher than the model prediction. Regarding these discrepancies between the data and our model, there are several possibilities: (i) the orbital modulation and the existence of the anisotropic stellar photon fields result in the TeV emission signal attenuating at this point in the phase; this is consistent with recent observational campaigns, i.e. no emission signature close to the periastron passage (Albert et al. 2006; Albert et al. 2008; Albert et al. 2009). (ii) the observed Chandra X-ray signatures do not correspond to the emission at this phase, but rather to the point around the periastron passage. (iii) the radio emission region is not from the studied regime; it may correspond to the termination region of jets (for a similar study, see Zhang & Feng 2010). On the other hand, the re-accelerated processes of secondary pairs may provide enough radio emission fluxes.

As seen in Figure 4, at phase 0.775, the model can approximately reproduce the simultaneous Chandra X-ray and TeV observations, but clearly it does not fit radio or *Fermi* LAT data. It is very possible that there is one population of particles producing the radio emission and a different one producing the observed X-ray and TeV emissions. Recent observations also show that there exists a possible hint of temporal correlation between the X-ray and TeV emissions as well as evidence for radio and TeV non-correlation (Albert et al. 2008). Very recently, Anderhub et al. (2009) have detected a simultaneous outburst at X-ray and TeV energies with the peak at orbital phase 0.62; it is

very near to the apastron passage (i.e. 0.775) (Aragona et al. 2009). In this work, we only calculate the emissions in LS I + 61 303 at the INFC and apastron passage (see also Fig. 2 for the superior conjunction). However, a detailed calculation covering the whole orbital phase is required to explain the discrepancies. Generally speaking, the results of numerical computations can roughly explain these emission phenomena; meanwhile, the results imply that emission processes at X-ray and TeV wavelengths could simultaneously take place. Moreover, it is very likely that a hadronic origin can operate in this source based on p-p interactions.

Alternatively, the soft X-ray emissions can also be explained by the thermal Comptonization of soft radiation from the accretion disk (e.g. Reig et al. 2003; Giannios 2005). It should be pointed out that we do not consider emission from the secondary pairs created by the γ-γ interaction processes, which has been studied in the hadronic dominated jet model framework (e.g. Romero et al. 2005; Orellana et al. 2007; Zhang et al. 2010).

In conclusion, we have adopted the parameterized formulae of the p-p interaction processes (Kamae et al. 2006) to obtain the secondary SEDs, including the high-energy photon spectrum from π^0 decay and the energy spectra of electrons and positrons. Then, adopting the up-to-date geometry of an elliptical orbit found in the literature (Aragona et al. 2009), we considered the orbital modulation due to the effects of different accretion rates, a variation of stellar wind ions, soft photon density at different orbital phases, and the orbital-phase and angular dependent γ-photon absorption. Finally, we obtained a multiwavelength photon spectrum for the microquasar LS I + 61 303. The resulting model can approximately reproduce the latest quasi-simultaneous observational data and the non-simultaneous multiband observations. Moreover, the model implies that the emissions at X-ray and TeV energies could originate from the primary protons.

Acknowledgements We thank Ying Chen for a critical reading of the manuscript. We would also like to thank an anonymous referee for the valuable comments and suggestions that helped to significantly improve this manuscript. This work is partly supported by the Guizhou provincial Natural Science Foundation (Nos. 08097 and 2010080), the National Natural Science Foundation of China (NSFC, Grant Nos. 10778702 and 10803005) and the National Basic Research Program of China (973 project 2009CB824800).

References

Abdo, A. A., et al. 2009, ApJ, 701, L123
Albert, J., et al. 2006, Science, 312, 1771
Albert, J., et al. 2008, ApJ, 684, 1351
Albert, J., et al. 2009, ApJ, 693, 303
Anderhub, H., et al. 2009, ApJ, 706, L27
Aragona, C., McSwain, M. V., Grundstrom, E. D., Marsh, A. N., Roettenbacher, R. M., Hessler, K. M., Boyajian, T. S., & Ray, P. S. 2009, ApJ, 698, 514
Araudo, A. T., Bosch-Ramon, V., & Romero, G. E. 2009, A&A, 503, 673
Blumenthal, G. R., & Gould, R. J. 1970, Reviews of Modern Physics, 42, 237
Bosch-Ramon, V., Romero, G. E., & Paredes, J. M. 2006a, A&A, 447, 263
Bosch-Ramon, V., Paredes, J. M., Romero, G. E., & Ribó, M. 2006b, A&A, 459, L25
Bosch-Ramon, V., & Khangulyan, D. 2009, International Journal of Modern Physics D, 18, 347
Böttcher, M., & Dermer, C. D. 2005, ApJ, 634, L81
Casares, J., Ribas, I., Paredes, J. M., Martí, J., & Allende Prieto, C. 2005, MNRAS, 360, 1105
Chernyakova, M., Neronov, A., & Walter, R. 2006, MNRAS, 372, 1585
Christiansen, H. R., Orellana, M., & Romero, G. E. 2006, Phys. Rev. D, 73, 063012
Dolag, K., & Enßlin, T. A. 2000, A&A, 362, 151
Dubus, G. 2006, A&A, 451, 9

Falcke, H., & Biermann, P. L. 1995, A&A, 293, 665
Frail, D. A., & Hjellming, R. M. 1991, AJ, 101, 2126
Giannios, D. 2005, A&A, 437, 1007
Gregory, P. C., & Neish, C. 2002, ApJ, 580, 1133
Gregory, P. C. 2002, ApJ, 575, 427
Gupta, S., & Böttcher, M. 2006, ApJ, 650, L123
Jamil, O., Fender, R. P., & Kaiser, C. R. 2010, MNRAS, 401, 394
Kamae, T., Karlsson, N., Mizuno, T., Abe, T., & Koi, T. 2006, ApJ, 647, 692
Kelner, S. R., Aharonian, F. A., & Bugayov, V. V. 2006, Phys. Rev. D, 74, 034018
Körding, E. G., Fender, R. P., & Migliari, S. 2006, MNRAS, 369, 1451
Marti, J., & Paredes, J. M. 1995, A&A, 298, 151
Martocchia, A., Motch, C., & Negueruela, I. 2005, A&A, 430, 245
Massi, M., Ribó, M., Paredes, J. M., Garrington, S. T., Peracaula, M., & Martí, J. 2004, A&A, 414, L1
Mirabel, I. F., & Rodríguez, L. F. 1999, ARA&A, 37, 409
Orellana, M., Bordas, P., Bosch-Ramon, V., Romero, G. E., & Paredes, J. M. 2007, A&A, 476, 9
Reig, P., Kylafis, N. D., & Giannios, D. 2003, A&A, 403, L15
Romero, G. E., Torres, D. F., Kaufman Bernadó, M. M., & Mirabel, I. F. 2003, A&A, 410, L1
Romero, G. E., Christiansen, H. R., & Orellana, M. 2005, ApJ, 632, 1093
Romero, G. E., Okazaki, A. T., Orellana, M., & Owocki, S. P. 2007, A&A, 474, 15
Romero, G. E., & Vila, G. S. 2008, A&A, 485, 623
Sidoli, L., Pellizzoni, A., Vercellone, S., Moroni, M., Mereghetti, S., & Tavani, M. 2006, A&A, 459, 901
Strickman, M. S., Tavani, M., Coe, M. J., Steele, I. A., Fabregat, J., Marti, J., Paredes, J. M., & Ray, P. S. 1998, ApJ, 497, 419
van Dijk, R., et al. 1996, A&A, 315, 485
Zhang, J.-F., Zhang, L., & Fang, J. 2009, PASJ, 61, 949
Zhang, J. F., Feng, Y. G., Lei, M. C., Tang, Y. Y., & Tian, Y. P. 2010, MNRAS, 407, 2468
Zhang, J. F., & Feng, Y. G. 2011, MNRAS, 410, 978